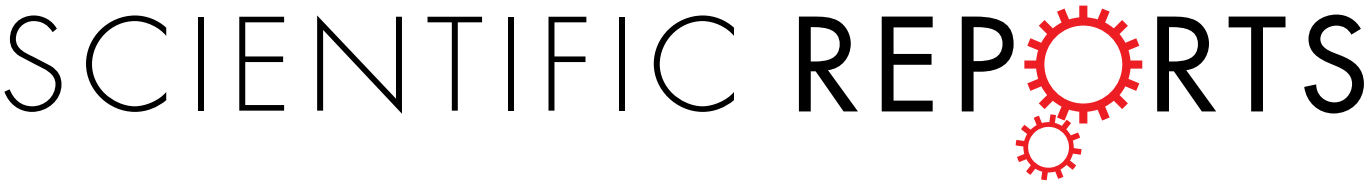

OPEN

Atom Probe Tomographic Imaging of PbS Quantum Dot Formation on Neodymium Clusters in Silicate Glasses

Received: 13 July 2018
Accepted: 27 June 2019
Published online: 11 July 2019

Won Ji Park, Ju Eun Kim, Ho Jeong Lee, Chan Gyung Park & Jong Heo

The first 3-D direct observation of clusters of Nd oxide inside silicate glasses was achieved using atom probe tomography. Three-dimensional elemental maps of major chemical elements in glasses such as Si, Al, Zn and O showed no evidence of regions that had concentrations higher than the average values, whereas the Nd aggregated into regions of high concentration. Elemental maps of Nd and Pb recorded from the glasses containing PbS QDs showed highly-concentrated areas of both elements at the same locations; this result indicates that PbS QDs formation started in association with the Nd clusters.

Rare-earth (RE)-doped glasses have been commercially used as signal amplifiers for optical communication and solid-state lasers that exploit the radiative f-f electronic transitions of trivalent RE ions[1–5]. One of the fundamental difficulties associated with emission by RE ions is that when RE ions assemble into clusters, concentration quenching occurs, in which neighboring ions exchange energy non-radiatively[6–9]. Many spectroscopic analyses have provided indirect evidence of RE clustering[10,11] but direct observation has not been reported.

Quantum dots (QDs) can provide emissions from mid-infrared to visible wavelength[12–19]. The optical and electronic properties of QDs depend on their size, so many attempts to realize the precise control of QDs size[20–26] have been reported. In particular, in glasses that include RE ions, QDs form near clusters of RE oxides that appeared to provide nucleation sites[27–29]. Distribution of elements analyzed from electron energy loss spectroscopy (EELS) suggested the presence of RE clusters. However, direct evidence of the presence of the RE-oxide clusters in conventional oxide glass is lacking, and their functions in nucleation of QDs in glasses are not known.

Atom probe tomography (APT) can provide single-atom sensitivity and fine spatial resolution (~0.1 nm in depth) of the distribution of chemical elements in three dimensions[30,31]. Local electrode atom probe (LEAP) uses an additional electrode to reduce the laser damage during analyses of insulating materials. Statistical tools including iso-surface image and maximum separation method can provide additional means to detect clusters or ordered phases with sizes smaller than a few nanometers[32,33]. We have employed APT to visualize the presence of RE clusters in silicate glasses. We also propose how RE clusters affect nucleation and growth of QDs in glasses.

Results

Specimen preparation using a dual beam focused ion beam method. Specimens for APT analysis were prepared by a dual-beam focused ion beam (FIB; FEI, Helios Nano-Lab 650) method using the standard lift-out technique designed for insulating materials (Fig. 1)[34–36]. First, Pt coating was sputtered (CRESSINGTON SPUTTER COATER 208HR) on the surface of glass specimens to avoid surface damage by Ga^+ ions (Fig. 1a). Then a thin slice of the specimen was lifted out of bulk glass material by several successive Ga^+ ion-beam millings, including trench milling of H-beam type (Fig. 1b). This specimen with ~2-μm width was repositioned on the tungsten tip (Fig. 1c) and further milled into a needle shape (Fig. 1d) with diameter of ~40 nm and length of ~80 nm, that was finally loaded into the atom probe (Fig. 1e).

Three-dimensional elemental mapping and computational analyses. First, APT analysis was performed on as-prepared glass with the composition $50SiO_2$–$5Al_2O_3$–25NaO–10BaO–8ZnO–2ZnS–0.8PbO–$5Nd_2O_3$ (in mol%). In tomographic reconstructions (Fig. 2), all elements (Si, O, Zn, Al, S and Pb; Fig. 2a–f) except

Department of Materials Science and Engineering, Pohang University of Science and Technology (POSTECH), Pohang, Gyeongbuk, 37937, Republic of Korea. Correspondence and requests for materials should be addressed to J.H. (email: jheo@postech.ac.kr)

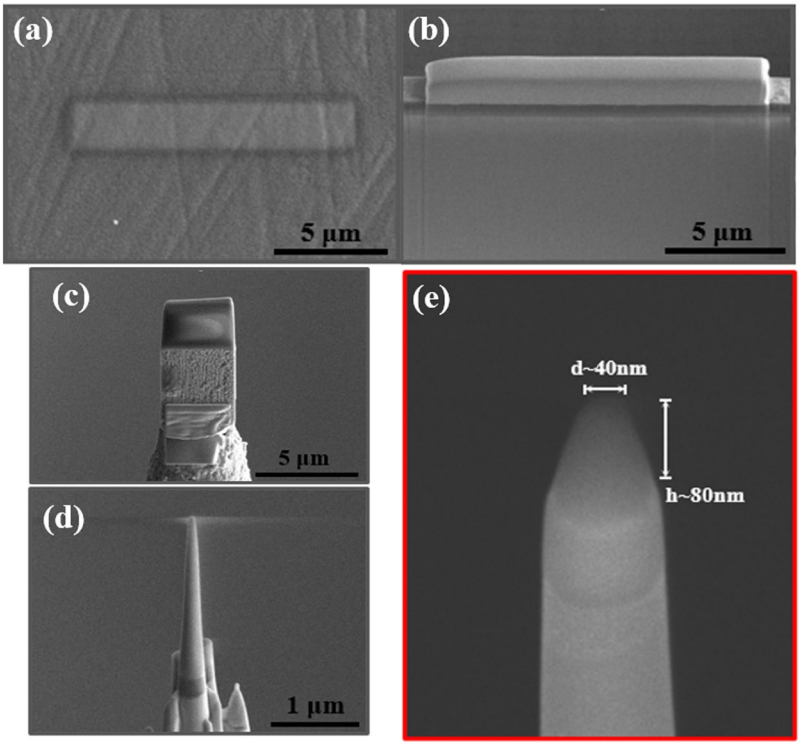

Figure 1. Procedures for preparation of tip-shaped glass specimen by using focused ion beam (FIB; FEI, Helios Nano-Lab 650) milling. (**a**) Pt deposition (~15 μm in length) to protect the surface of the specimen, (**b**) Cross-section view of a thin slab detached from the glass specimen, (**c**) Glass thin slab attached to tungsten tip, (**d**) Further milling into a needle shape, (**e**) Final specimen with 40-nm diameter and 80-nm length.

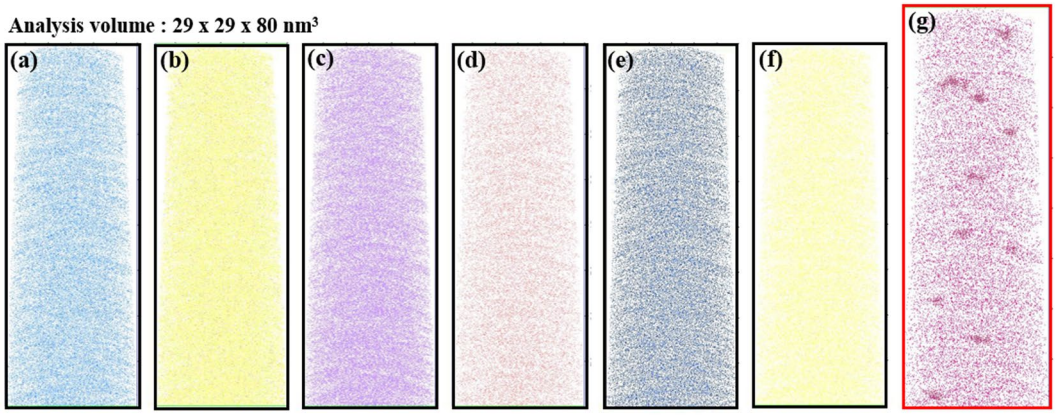

Figure 2. Three-dimensional elemental distribution maps for (**a**) Si, (**b**) O, (**c**) Zn, (**d**) Al, (**e**) S, (**f**) Pb and (**g**) Nd atoms. Volumes of glass used for analyses were ~29 × 29 × 80 nm. Every dots corresponds to each atom and the position of an atom represents the actual location in the glass matrix.

Nd (Fig. 2g) were distributed homogeneously. Nd concentration ([Nd]) was high in many regions. This is the first visual three-dimensional (3D) mapping of RE clusters in a glass. Clustering of RE ions in solid matrices has been considered as a major source of the energy transfers that degrade the emission efficiencies of REs. For example, fluorescence intensity of the Tb^{3+}: $^5D_3 \rightarrow {}^7F_5$ transition decreases as [Tb^{3+}] in the glass increases[37]. Indirect evidence such as decrease in fluorescent lifetimes and fluorescent intensities of RE ions at certain energy levels have been used to propose the presence of clustering, but this is the first 3-D direct observation of regions with RE ion concentration higher than those expected from the homogeneous distribution.

We further performed computational analysis using the iso-surface imaging method to visualize areas of high [Nd] clearly. The 1.40% Nd-iso surface analysis shows clear images of Nd-rich regions inside the matrix (Fig. 3a). A similar analysis for Si did not reveal any images of clustered areas, because Si was distributed homogeneously in the specimen so the analysis did not form a closed surface (Fig. 3b). The elemental concentration profile (Fig. 3c)

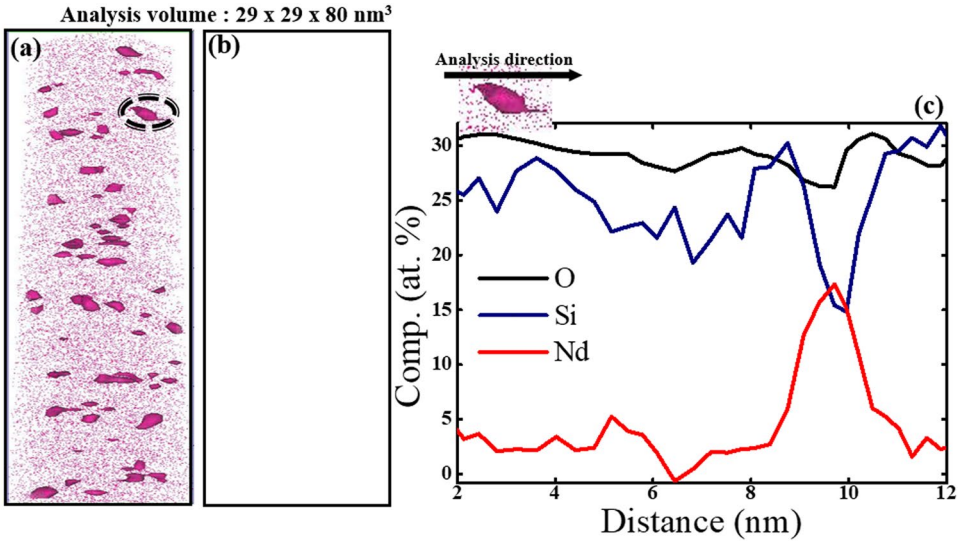

Figure 3. Isolated atom distribution image of (**a**) Nd and (**b**) Si obtained from the iso-surface analysis with 1.40 at.% each atom. (**c**) Concentration profile of each element (Si, O, Nd) in a cluster of ~3-nm diameter.

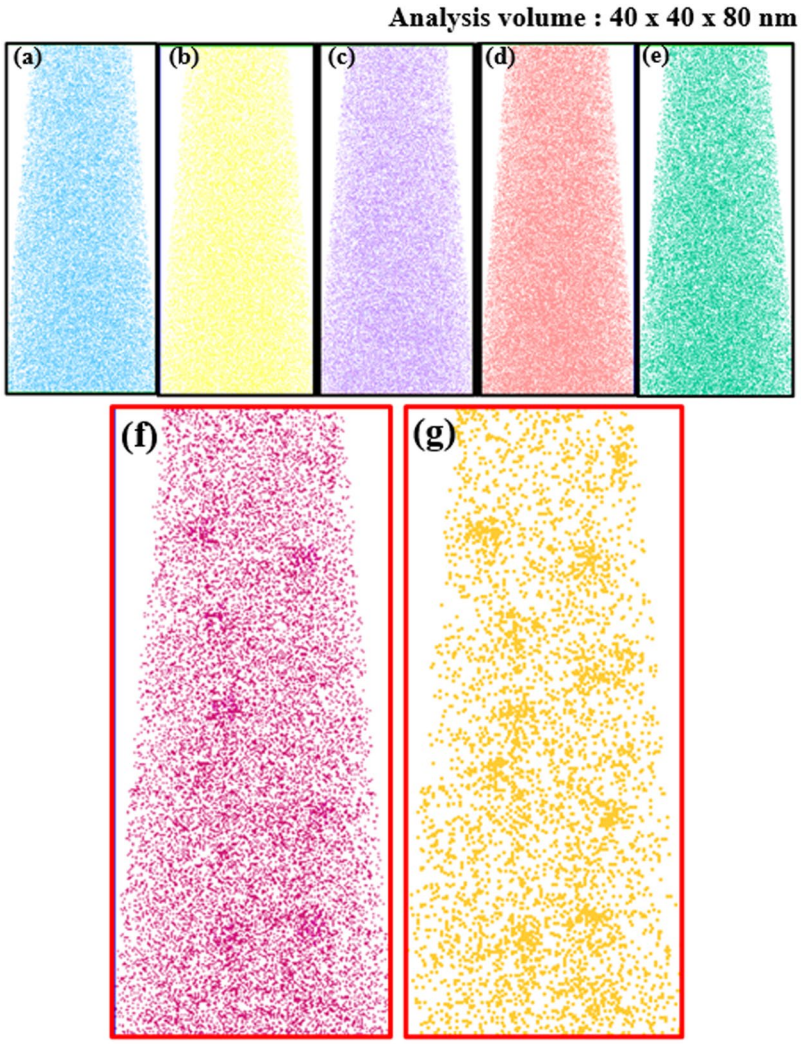

Figure 4. Three-dimensional elemental distribution maps for (**a**) Si, (**b**) O, (**c**) Zn, (**d**) Al (**e**) S, (**f**) Nd and (**g**) Pb atoms in glasses after heat treatment at 500 °C for 30 h. Volumes of glass used for analyses were ~40 × 40 × 80 nm.

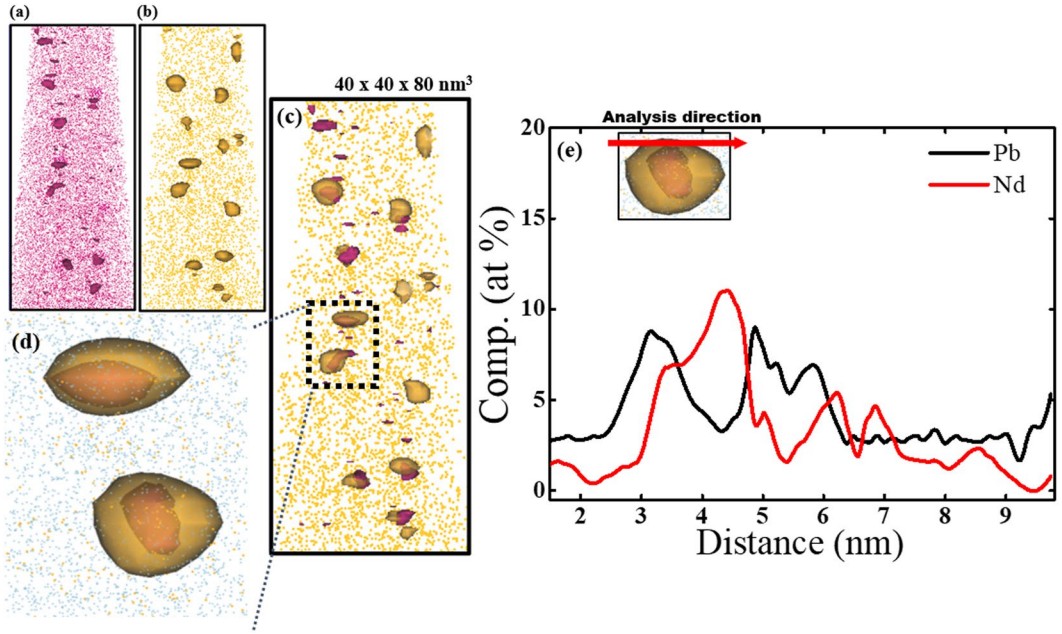

Figure 5. Isolated atom distribution image obtained from iso-surface concentration analyses of (**a**) Nd with 1.40 at.% Nd, (**b**) Pb with 1.40 at.% Pb and (**c**) graphical combination of (**a**,**b**). (**d**) Magnified image of two PbS QDs in (**c**,**e**) concentration profiles of Pb and Nd in a QDs with ~4-nm diameter.

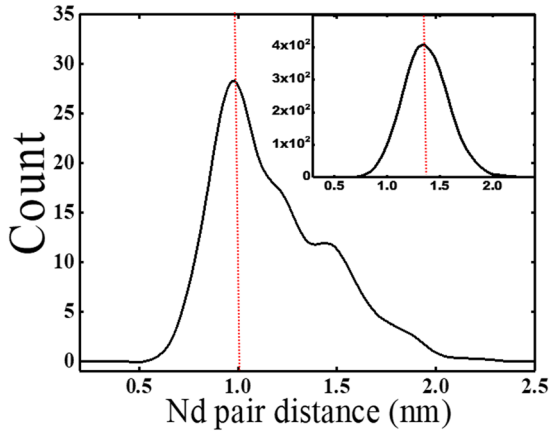

Figure 6. First nearest neighbor (1NN) distance D_{max} distribution of Nd inside clusters to obtain the value of D_{max} for the maximum separation method. Inset: 1NN distance of Nd in glass matrix.

recorded from one Nd cluster indicated that [Nd] atoms increased to ~18 at.% across ~3 nm in diameter. [Si] in the cluster decreased, but [O] remained constant at ~30 at.%.

Afterwards, glass was heat-treated at 500 °C for 30 h to precipitate PbS QDs. 3D distributions (Fig. 4a) of each element were obtained from a volume of approximately 40 × 40 × 80 nm in silicate glass containing 5.0 mol.% Nd_2O_3. Most of the elements (e.g., Si, O, Zn, Al, S atoms) that form the glass matrix were uniformly distributed (Fig. 4a–e). Some clustered areas had high [Nd] (Fig. 4f) and high [Pb] (Fig. 4g), but some Nd and Pb remained in the glass matrix. Regions of high [Nd] concentration (Fig. 4f) appear to overlap regions of high [Pb] (Fig. 4g).

We also conducted iso-surface compositional analyses for areas of clustered Nd and Pb. Results of the analyses with 1.40% Nd iso-surface concentration contour showed Nd-rich regions (Fig. 5a) similar to those in Fig. 3a. In addition, areas with high [Pb] (i.e., PbS QDs) were detected in glasses (Fig. 5b). In the same analysis, Si and Al atoms did not show clustering. Combination of Fig. 5a,b proved that Nd clusters almost coincide with the location of PbS QDs (Fig. 5c); this result suggests that the growth of PbS QDs is closely related to the presence of Nd clusters (Fig. 5d) and it is consistent with the results of electron energy loss spectroscopy (EELS) (Fig. S1)[28]. The elemental concentration profile along one QD showed that [Pb] increased to ~10 at.%, and [Nd] increased to 12 at.% (Fig. 5e).

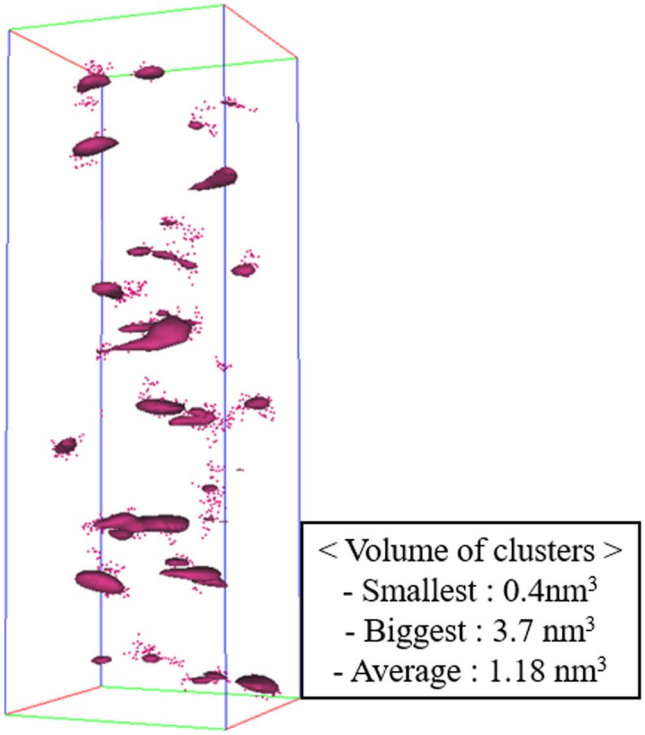

Figure 7. Analyzed Nd clusters by maximum separation algorithm with appropriate parameters. Inset table: compositional difference between clusters and glass matrix.

Nd cluster analysis using the maximum separation method. We visualized Nd clusters in 3D elemental mapping (Fig. 2) and iso-surface images (Fig. 3). We also used the maximum-separation method. The value of χ^2 is usually determined from the distribution of Nd inside the matrix: $\chi^2 = 0$ suggests a random distribution; $\chi^2 > 0$ indicate that clusters exist[38–40]. The glass specimen that contained 5.0 mol.% of Nd_2O_3 had χ^2 ~0.93 before heat treatment. This result is another evidence of a non-uniform and heterogeneous distribution of Nd in the glass matrix.

Afterwards, the Nd-Nd nearest-neighbor analysis between cluster and matrix was obtained from Fig. 6 to determine the nearest neighbor distance D_{max} between Nd atoms. Evaluation considered 14471 blocks of 100 atoms. D_{max} was ~1.0 nm in the clusters ~1.5 nm in the glass matrix. Other parameters considered are *Order*, which is the number of nearest Nd atoms around a specific Nd atom; N_{min}, which is the minimum size of cluster that can be considered as a cluster; and *E*, which is the erosion distance at which an atom can be considered to have moved from the cluster to the matrix[41]. Numbers used for the cluster analysis were $D_{max} = 1.0$, $Order = 6$, $N_{min} = 10$ and $E = 1.0$ nm; analysis detected 81 Nd clusters in Fig. 7a, with volumes of 0.40–3.7 nm^3 (average 1.18 nm^3). Average [Nd] within the clusters was 56.3 at.%, which is ~19 times higher than the average [Nd] = 3.3 at.% in the glass matrix.

Nd^{3+} ions are surrounded by an average of seven oxygens both before and after the formation of PbS QDs in glasses[29]. Therefore, clusters of high [Nd] (Figs 2 and 4) are most probably made of NdO_x polyhedra rather than of Nd-Nd bonds. Precipitation of PbS QDs occurs in association with Nd-O clusters.

We have demonstrated the presence of Nd clusters in silicate glasses by using atom probe tomography and 3D elemental mapping. Distributions of the major chemical elements that constitute the (e.g., Si, Al, O) showed no evidence clustering. When the glasses were heat-treated at 500 °C for 30 h to precipitate the PbS QDs, areas of high [Nd] and [Pb] formed in the glasses, and closely coincide with each other; this result indicates that formation of PbS QDs most probably started at the Nd clusters.

Method

Glass preparation. A base glass with a nominal composition of $50SiO_2$–$5Al_2O_3$–25NaO–10BaO–8ZnO–2ZnS–0.8PbO (in mol%) and a Nd-glass with an additional 5 mol% of Nd_2O_3 were prepared using a conventional melt-quenching process. Starting powders were mixed and melted in an alumina crucible at 1340 °C for 30 min. Each melt was poured onto a brass mold that had been preheated at 380 °C, then was quenched by pressing with another brass plate. Resulting glasses were annealed at 380 °C for 2 h to eliminate residual thermal stress. Specimens were polished to ~150-μm thickness, then used as a source for fabrication by FIB of specimens for APT.

Atom Probe Tomography (APT). APT analysis (CAMECA, LEAP4000X HR) was performed using a pulsed UV laser ($\lambda = 355$ nm) and each atom was detached from the surface by irradiating the laser beam with

100-pJ pulse energy at a repetition rate of 200 kHz. An additional local electrode with a range of 2–15 kV was used to avoid the specimen damage by the laser beam. IVAS software (3.6.10a version) by CAMECA Instruments was used to reconstruct and visualize APT results. Cluster formation was identified from the iso-surface concentration. The maximum-separation algorithm was used to distinguish the clusters from the matrix, and the corresponding differences between the matrix and cluster compositions were calculated.

References

1. Kotani, A. *et al*. Theory of core-level spectroscopy of rare-earth oxids. *J. Electron. Spectrosc. Relat. Phenom.* **60**, 257–99 (1992).
2. Mozian, V. *et al*. Er^{3+}-doped GeGaSbS glasses for mid-IR fibre laser application: Synthesis and rare earth spectroscopy. *Opt. Mater.* **31**, 39–46 (2008).
3. Chu, Z. *et al*. Water-vapor absorption line measurements in the 940-nm band by using a Raman-shifted dye laser. *Appl. Opt.* **32**, 992–8 (1993).
4. Campbell, J. *et al*. Nd-doped phosphate glasses for high-energy/high-peak power lasers. *J. Non-Cryst. Solids* **263**, 318–41 (2000).
5. Yamanaka, C. *et al*. Nd-doped phosphate glass laser systems for laser fusion research. *IEEE J. Quantum Electron.* **17**, 1639–49 (1981).
6. Arai, K. *et al*. Aliminium or phosphorus co-doping effects on the fluorescence and structural properties of neodymium-doped silica glass. *J. Appl. Phys.* **59**, 3430–6 (1986).
7. Ainslie, B. J. *et al*. Optical and structural investigation of Nd^{3+} in silica-based fibers. *J. Mater. Sci. Lett.* **6**, 1361–3 (1987).
8. Morkel, P. R. *et al*. Spectral variation of excited state absorption in neodymium doped fiber lasers. *Opt. Commun.* **67**, 349–52 (1988).
9. Aitken, B. G. *et al*. Clustering of rare earths in GeAs sulfide glass. *C. R. Chimie* **5**, 865–72 (2002).
10. Monreil, A. *et al*. Clustering of rare earth in glasses, aluminum effect: experiments and modeling. *J. Non-Cryst. Solids* **348**, 44–50 (2004).
11. Mizoguki, T. *et al*. Atomic-Scale Identification of Individual Lanthanide Dopants in Optical Glass Fiber. *ACS nano* **7**, 5058–63 (2013).
12. Bakueva, L. *et al*. Size-tunable Infrared (1000–1600 nm) Electroluminescence from PbS Quantum-dot Nanocrystals in a Semiconducting Polymer. *Appl. Phys. Lett.* **82**, 2895–7 (2003).
13. Steckel, J. S. *et al*. 1.3 μm to 1.55 μm Tunable Electroluminescence from PbSe Quantum Dots Embedded Within Organic Device. *Adv. Mater.* **15**, 1862–6 (2003).
14. Kamat, P. V. Quantum Dot Solar Cells. Semiconductor Nanocrystals as Light Harvesters. *J. Phys. Chem. C* **112**, 18737–53 (2008).
15. Kamat, P. V. Meeting the Clean Energy Demand: Nanostructure Architectures for Solar Energy Conversion. *J. Phys. Chem. C* **111**, 2834–60 (2007).
16. Colvin, V. L. *et al*. Light-emitting diodes made from cadmium selenide nanocrystals and a semiconducting polymer. *Nature* **370**, 354–7 (1994).
17. Sullivan, S. C. *et al*. Tuning the performance of hybrid organic/inorganic quantum dot light-emitting devices Org. *Eletron.* **4**, 123–30 (2003).
18. Tittel, J. *et al*. Fluorescence Spectroscopy on Single CdS Nanocrystals. *J. Phys. Chem. B* **101**, 3013–6 (1997).
19. Wang, Y. *et al*. Nanometer-Sized Semiconductor Clusters: Materials Synthesis, Quantum Size Effects, and Photophysical Properties. *J. Phys. Chem.* **95**, 525–32 (1991).
20. Liu, C. *et al*. Laser-induced blue-shift of the photoluminescence from PbS quantum dots in glasses. *Chem. Phys. Lett.* **452**, 281–4 (2008).
21. Moreels, I. *et al*. Size-Dependent Optical Properties of Colloidal PbS Quantum Dots. *ACS Nano* **3**, 3023–30 (2009).
22. Liu, C. *et al*. Photoluminescence of PbS quantum dots embedded in glasses. *J. Non-Cryst. Solids* **354**, 618–23 (2008).
23. Heo, J. *et al*. PbS quantum-dots in glass matrix for universal fiber-optic amplifier. *J. Mater. Sci.: Mater. Electron.* **18**, S135–9 (2007).
24. Shim, S. M. *et al*. Lead Sulfide Quantum Dots Formation in Glasses Controlled by Erbium Ions. *J. Am. Ceram. Soc.* **93**, 3092–4 (2010).
25. Xu, K. *et al*. Influence of silver nanoclusters on formation of PbS quantum dots in glasses. *J. Non-Cryst. Solids* **357**, 2428–30 (2011).
26. de Lamaestre, R. E. *et al*. Synthesis of Lead Chalcogenide Nanocrystals by Sequential Ion Implantation in Silica. *J. Phys. Chem. B* **109**, 19148–55 (2005).
27. Kim, M. A. *et al*. Lead Sulfide Quantum Dots in Glasses Containing Rare Earth Ions. *J. Non-Cryst. Solids.* **383**, 173–5 (2014).
28. Park, W. J. *et al*. Direct Imaging of the Distribution of Nd^{3+} ions in Glasses Containing PbS Quantum Dots. *J. Am. Ceram. Soc.* **98**, 2074–7 (2015).
29. Park, W. J. *et al*. Role of Nd^{3+} ions on the nucleation and growth of PbS quantum dots (QDs) in silicate glasses. *J. Am. Ceram. Soc.* **100**, 2879–84 (2017).
30. Muller, E. W. *et al*. Atom-Probe Field Ion Microscope. *Rev. Sci. Instrum.* **39**, 83–6 (1968).
31. Cerezo, A. *et al*. Atom probe tomography today. *Mater. Today* **10**, 36–42 (2004).
32. Tsong, T. Atom-Probe Field-Ion Microscopy. Cambridge Univ. *Press* (1990).
33. Miller, M. K. *et al*. Atom probe tomography of nanoscale particles in ODS Ferritic alloys. *Mater. Sci. Eng.* **353**, 140–5 (2003).
34. Kelly, T. F. *et al*. Invited review article: Atom probe tomography. *Rev. Sci. Instrum.* **78**, 031101–20 (2007).
35. Seidman, D. N. Three-dimensional atom-probe tomography: Advances and applications. *Annu. Rev. Mat. Res.* **37**, 127–58 (2007).
36. Miller, M. K. Materials science - Imaging elusive solute atoms. *Science* **286**, 2285–6 (1996).
37. Tonooka, K. *et al*. A non-linear analysis of energy transfer in highly Tb^{3+}-doped glasses. *J. Lumin.* **50**, 139–51 (1991).
38. Blavette, D. *et al*. An Atom-Probe for 3-Dimensional Tomography. *Nature* **363**, 432–5 (1993).
39. Marquis, E. A. *et al*. Applications of atom-probe tomography to the characterization of solute behaviors. *Mat. Sci. Eng. R* **69**, 37–62 (2010).
40. Williams, C. A. *et al*. Defining clusters in APT reconstructions of ODS steels. *Ultramicroscopy* **132**, 271–8 (2013).
41. Thompson, K. *et al*. *In-situ* site-specific specimen preparation for atom probe tomography. *Ultramicroscopy* **107**, 131–9 (2007).

Acknowledgements

This research was supported by a Basic Science Research Program (NRF-2017M2B2B1072405) through the National Research Foundation (NRF) funded by the Ministry of Science and ICT, Korea.

Author Contributions

J. Heo conceived and coordinated the research project. W.J. Park designed the glass compositions and prepared the specimens and H.J. Lee conducted TEM and the compositional analysis. J.E. Kim performed APT measurement and C.G. Park guided J.E. Kim for the cluster analyses. All authors participated in discussion and manuscript preparation.

Additional Information

Supplementary information accompanies this paper at https://doi.org/10.1038/s41598-019-46574-1.

Competing Interests: The authors declare no competing interests.

Publisher's note: Springer Nature remains neutral with regard to jurisdictional claims in published maps and institutional affiliations.